Springer

KSME

Journal of Mechanical Science and Technology 30 (3) (2016) 1431~1442
www.springerlink.com/content/1738-494x(Print)/1976-3824(Online)
DOI 10.1007/s12206-016-0251-1

Numerical study of conjugate heat transfer of steam and air in high aspect ratio rectangular ribbed cooling channel †

Tieyu Gao*, Jiangnan Zhu, Changwei Liu and Jiamin Xu

Institute of Turbomachinery, School of Energy & Power Engineering, Xi'an Jiaotong University, Xi'an, 710049, Shaanxi, China

(Manuscript Received July 7, 2015; Revised September 17, 2015; Accepted September 28, 2015)

Abstract

The relationship between flow field and heat transfer in an air/steam cooled ribbed channel was numerically investigated and compared. The width to height ratio was 4 and the rib height to hydraulic diameter was 0.078. The conjugate heat transfer method was adopted and a uniform heat source was located in the solid domain to simulate the actual heating method in the experiment. The GGI method was used to deal with the solid-fluid interface. The fluid field structure was shown by vortex core technology. We found that the wall heat flux distribution is similar with that of the Nusselt number, which is periodic. The temperature difference of a certain position on the inner and outer wall was less than 2 K. The Nusselt number reached its peak value at No.15-18 part and then decreased. The large width to height ratio led to strong interaction between the main flow fluid and the fluid in near wall region. As a result, an extra main flow secondary flow and two separation vortexes could be observed. These three additional vortexes were all in main flow region. The two separation vortexes approached to each other in flow direction and mixed into one vortex at low Reynolds number. When Reynolds number is larger than 30000, the two vortexes remain independent. The relative distance between them reaches the minimum value and the Nusselt number reaches the peak value at the same time. In addition, the flow field structure is mainly determined by Reynolds number and the fluid type cannot obviously influence the secondary flow distribution. The generation and separation of secondary flow as well as the mixing of secondary flows can enhance the local heat transfer strength.

Keywords: Conjugate heat transfer; Gas turbine; Internal cooling; Secondary flow vortex core

1. Introduction

Gas turbines have been widely used for land based power generation. The thermal efficiency of the engine can be improved by raising the turbine inlet temperature. However, doing so beyond the melting point of the metal components can result in component failure, leading to engine failure. As a result, a variety of cooling techniques have been widely used by the modern gas turbines. Among them, one method for cooling the blade is internal cooling. This technology pumps air from compressor to the internal ribbed passage to cool the material through heat convection between air and passage wall.

To enhance the heat convection strength of the cooling channel, ribs are located on the wall to cause the separation of boundary layer. By now, the parallel straight angled rib is still the most widely used rib structure in gas turbine blade cooling channels. Many investigations have been conducted to illustrate the heat transfer enhancement ability of this kind of rib. Han et al. [1-6] systematically investigated the heat transfer and flow characteristics of air in rectangular ribbed cooling channel and the effect of channel aspect ratio, heat flux ratio, rib angle and the ratio of rib space to rib height on heat transfer performance. Rau et al. [7] investigated the influence of ratio of rib space to rib height on the ribbed wall heat transfer performance. Kiml et al. [8] investigated the effect of rib height on the heat transfer and pressure loss characteristics of channel with 60° and 90° ribs. Liu and Chung [9] simulated the air flow between the two ribs whose attack angle is 90° by large eddy simulation. The results indicated that the streamline reattached at x = 5h downstream after the first rib. Ryu et al. [10] investigated the flow field between two neighboring rectangular, triangular and semicircle ribs whose attack angle was 90°. The results showed that the space-averaged temperature profile exhibited a logarithmic region with a heat-transfer roughness function that varied with a constant power of the roughness Reynolds number. A log region existed in the space-averaged temperature profile for all cases. Leonardi et al. [11] studied the flow field of air in ribbed channels using Direct numerical simulations (DNS). The flow field showed the influence of the ratio of rib height and rib spacing on flow structure. Schabacker et al. [12] measured the distribution of time-averaged velocity and turbulence intensity in the sharp

*Corresponding author. Tel.: +86 29 82664103, Fax.: +86 29 82664103
E-mail address: sunmoon@mail.xjtu.edu.cn
† Recommended by Associate Editor Ji Hwan Jeong

turn region by PIV method. Schüler et al. [13] studied the heat transfer characteristics and pressure loss in a two-pass rectangular cooling channel with 45° ribs. Liu et al. [14] experimentally studied the flow and heat transfer performance in the two-pass rectangular cooling channel with ribs and film holes. Liou et al. [15] measured the flow field of a 90° ribbed two-pass cooling passage and studied the corresponding heat transfer performance. Kubacki et al. [16] studied the vortex shape and distribution in rotating 90° ribbed cooling channel by vortex core technology.

The traditional air cooling method will cost a large amount of compressed air, which reduces the power output of the gas turbine. At the same time, the cooling effect of air is also facing limitation and the higher turbine inlet temperature requires a more effective cooling method. Since steam has a larger conductivity value, which means that steam may have larger cooling ability than air. As a result, it is very likely to replace air in the cooling of gas turbine blade. Corman [17] and Fukue [18] investigated the advantages of steam cooling and its contribution to the improvement of combined-cycle efficiency. Facchini et al. [19] studied the vane cooling performance of closed steam cooling technology and air cooling technology. The result showed that steam needs only 50% of the same flow rate as air to get the same cooling performance, and steam-air semi-closed cooling method can make the temperature distribution of the blade more uniform. Sanjay et al. [20] studied the thermal efficiency of gas turbine which adopted steam cooling and air cooling. The results showed that the thermal performance of gas turbine which adopted steam cooling technology was largely improved compared with the gas turbine which used air cooling. Kumar et al. [21] studied the thermal efficiency of gas turbine which adopted the steam cooling and air cooling. The results show that the cycle thermal efficiency of steam cooling gas turbine is 2.58% higher than that of gas turbine which using air cooling. Nomoto et al. [22] simulated the real working conditions of the gas turbine blades in the experiment and studied the cooling performance of high-pressure steam flowing in the smooth round pipe and impingement cooling the first stator by medium-pressure steam. The results showed that steam cooling got an excellent effect in the first stator. Liu et al. [23-25] studied the flow and heat transfer characteristics of steam in the rectangular ribbed channels with different ducts aspect ratio and rib attack angle by experiments and obtained semi-empirical correlations between Nusselt number and Reynolds numbers. Shui et al. [26, 27] studied the influences of steam superheat degree and pressure on the flow and heat transfer performance in the 90° angle ribbed rectangular channels. Gong et al. [28, 29] compared the heat transfer performance of air and steam in the same cooling channel. Zhu et al. [30] investigated the distribution and shape of secondary flow vortex core in a straight rectangular (W/H = 1) steam-cooled channel with 45° ribs and analyzed the relationship between secondary flow and heat transfer enhancement.

The separation and reattachment of the boundary layer due to the influence of rib being more strongly affected by the main flow fluid in large aspect ratio passage compared with that in square ribbed channel. It is necessary to investigate the structure of fluid field and analyze the difference of air and steam in flow field structure and heat transfer performance. The current study focuses on the steam and air cooled gas turbine blade cooling channel. The fluid field structure is shown by vortex core technology. The shape and distribution of secondary flow vortex core can illustrate the internal relationship between the secondary flow and heat transfer strength and then provide the scientific basis for designers to better control and manage the flow in ribbed channels.

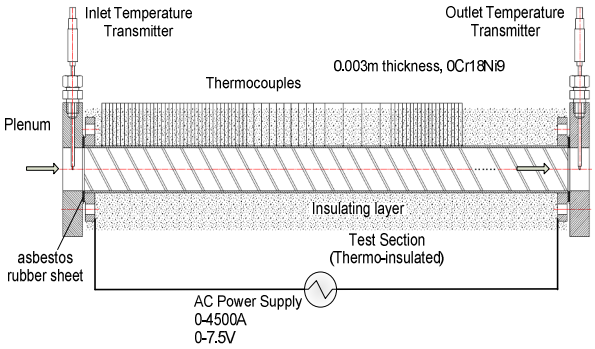

Fig. 1. The details of the test channel [29].

2. Description of the problem

2.1 Physical object and mesh generation

To investigate the heat transfer characteristics of steam and air in actual operation conditions, a new heating method is needed. The test was conducted on the multifunctional cooling test system of high-temperature turbine blade/vane with two coolants at Xi'an Jiaotong University, which was previously presented by Liu et al. [23-25] Shui et al. [26, 27] and Gong et al. [28, 29]. The test channel was stainless steel and the thickness of the channel wall was 3 mm, which is similar with the actual blade cooling channel. The Large-current and Low-voltage heating method was adopted. The test channel worked as the electric resistance. The maximum current of the heating device was 4500 A with maximum voltage of 7.5 V. All exterior surfaces of the test section were thermally insulated with 50 mm thickness aluminum silicate to minimize conduction heat losses to the environment. 50 E-Type thermocouples with an accuracy of ±1 K were welded on centerline of the outer surface of the ribbed wall. The thermocouples were placed on the outer surface of the channel ribbed wall in the region of $0.45 < Z/D < 9.95$. A Yokogawa MX100 data acquisition system was used for temperature reading and recordings. The maximum uncertainty in the Nusselt number was estimated to be less than 8% for Reynolds numbers larger than 10000 by using the uncertainties estimation method of Kline [31]. The maximum heat loss was estimated as 5% of total heat supply by the heat loss test.

Table 1. The geometry parameters of the channel.

W	H	e	D_h	P/e	α	L1	L
80 mm	20 mm	2.5 mm	32 mm	10	45°	8 mm	600 mm

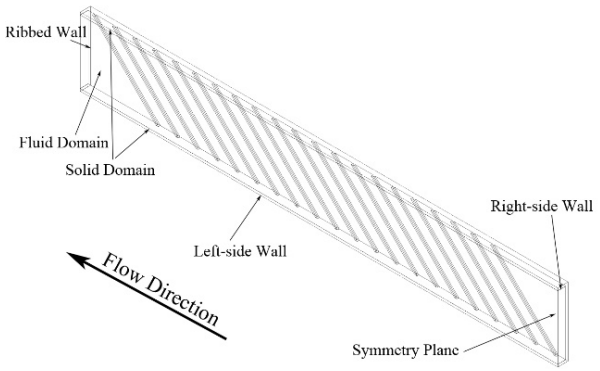

(a) The numerical model

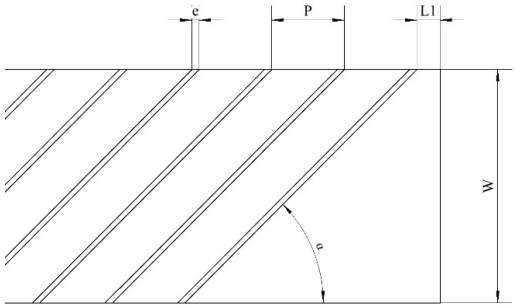

(b) The structure of the model (Top view of fluid domain)

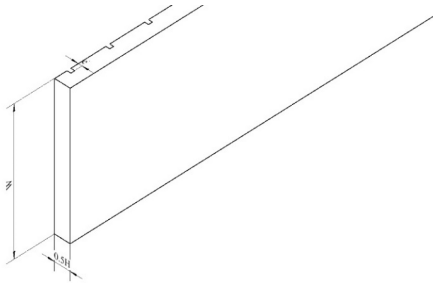

(c) The structure of the fluid domain (Axonometric view)

Fig. 2. Detailed description of the numerical model.

A numerical model was set up according to the test section in the experiment. To simulate the gradual heat transfer process in the experiment, we adopted the conjugate heat transfer method. A schematic diagram of the geometry is shown in Fig. 2 and its detailed parameters are shown in Table 1. Because only a 523 mm long section from the inlet plane was investigated in the experiment, the numerical model was set as 600 mm long to reduce the mesh number as well as avoid the influence of outlet on heat transfer.

Fig. 3(a) shows the mesh of the fluid domain and Fig. 3(b) shows the mesh of the solid domain. The fluid mesh is refined in the near wall region to make sure the y^+ value below 1 in every working condition. Since the node positions in solid

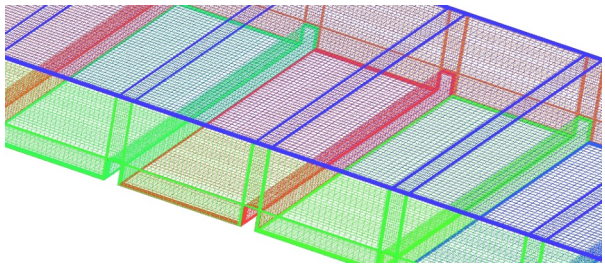

(a) Fluid domain mesh

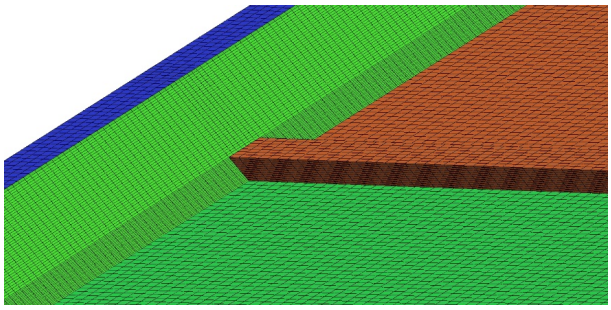

(b) Solid domain mesh

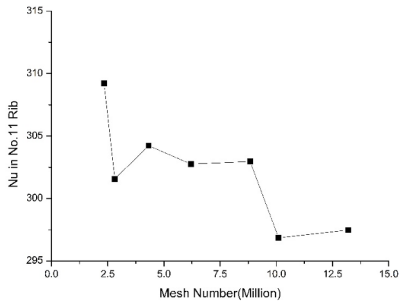

(c) Mesh independency test

Fig. 3. Mesh in (a) fluid domain; (b) solid domain; (c) mesh independency test.

domain and fluid domain are not corresponding, the GGI method was adopted to deal with the data transfer process through the interface of solid and fluid domain. To make the best use of computer resources, seven kinds of mesh numbers were tested to find the appropriate grid number, which is shown in Fig. 3(c). As a result, the mesh number of 10.1 million (1.89 million for solid and 8.21 million for fluid) was adopted in the numerical simulation.

2.2 Boundary condition and turbulence model

The fluid was set as Air ideal gas and steam (IAPWS-97) for the air case and steam case, respectively. The reference pressure of the fluid domain was set as 0.3 MPa. The static pressure and temperature were set at the inlet plane, which was 0 Pa and 447 K, respectively. A turbulence intensity of 15% was allocated at the inlet boundary to simulate the sudden-entrance inlet condition. The mass flow rate was set at the outlet boundary according to the corresponding Reynolds

numbers, which are 10000, 20000, 30000, 40000, 50000 and 60000, respectively, in this paper. A symmetry condition was set at the symmetrical plane of both the solid and fluid domain. The outer walls of the solid domain were set as adiabatic, and the contact surfaces between the solid and fluid domain were set as domain interface. The conservative interface flux condition was adopted for the heat transfer calculation on the interface. A uniform heat source was located in the solid domain to simulate the heating method in the experiment. The high resolution discrete scheme in the ANSYS CFX was adopted for the governing equations and turbulence model. The shear stress turbulence model, which has proven to be successful in the prediction of 45-deg ribbed rectangular cooling channel by Walker and Zausner [32], was adopted and the near-wall region was managed by the automatic wall function in the ANSYS CFX. The convergence criterion was set at 10^{-5} for the Root-mean-square (RMS) error.

2.3 Data reduction

The Reynolds number is computed by

$$\mathrm{Re} = \frac{\rho V D_h}{\mu} \tag{1}$$

where D_h is the hydraulic diameter of the channel, μ is the dynamic viscosity.

The local Nusselt number Nu is calculated by Eq. (2) and the Nusselt number in fully-developed turbulent nonrotating tube flow is computed by Eq. (3). The local heat transfer coefficient h is computed by Eq. (4). The value of Pr was set as 0.71 for air and 0.919 for steam in this study.

$$Nu = \frac{hD_h}{k} \tag{2}$$

$$Nu_0 = 0.023\,\mathrm{Re}^{0.8}\,\mathrm{Pr}^{0.4} \tag{3}$$

$$h = \frac{q}{T_w - T_b}. \tag{4}$$

2.4 Vortex core method

The ANSYS CFD-POST was adopted for the treatment of calculation results. The vortex core technology in CFD-POST was used for the study of the distribution and shape of swirling flow and vortex. Jeong and Hussain [33] studied the several different definitions of vortex core including the Local pressure minimum definition, the Q criterion and the $-\lambda_2$ definition. The accuracy and stability of these three criterions on the detection of vortices were compared. The results showed that the $-\lambda_2$ definition was the most accurate definition. So this definition was used in this paper and its detailed calculation method is shown below.

The velocity gradient tensor can be written as below:

$$D = \left[d_{ij} \right] = \begin{bmatrix} \frac{\partial u}{\partial x} & \frac{\partial u}{\partial y} & \frac{\partial u}{\partial z} \\ \frac{\partial v}{\partial x} & \frac{\partial v}{\partial y} & \frac{\partial v}{\partial z} \\ \frac{\partial w}{\partial x} & \frac{\partial w}{\partial y} & \frac{\partial w}{\partial z} \end{bmatrix}. \tag{5}$$

The tensors S and Ω are defined as below:

$$S = \frac{D + D^T}{2} \tag{6}$$

$$\Omega = \frac{D - D^T}{2}. \tag{7}$$

Then: $S + \Omega = D$, $S^2 + \Omega^2 = \mathrm{sym}(D^2)$.

According to Jeong and Hussain [33], the tensor $S^2 + \Omega^2$ determines the existence of a local pressure minimum due to vortical motion, and the connected region with two negative eigenvalues of $S^2 + \Omega^2$ can be the definition of vortex core. Because this tensor is a symmetric tensor, only the real eigenvalues can be obtained. If the three real Eigen-values are $\lambda_1 \geq \lambda_2 \geq \lambda_3$, then this vortex core definition is equivalent to $\lambda_2 < 0$, which was adopted in this study.

2.5 Validation of the numerical method

In Fig. 4, the numerical results are evaluated with the experiment results. It can be seen that the numerical result of the area-averaged Nusselt number on the ribbed wall matches with the experiment data to a reasonable value. Slight deviation exists when Re = 30000 and the fluid is air but the other data are closer in other working conditions. Hence, the numerical results are in good agreement with the experimental results.

3. Results and discussion

3.1 Gradual heat transfer characteristics

Fig. 5(a) shows the temperature distribution on the inner and outer surface of the ribbed wall. The temperature distributions on these two surfaces are similar. The high temperature region, which indicates poor heat convection strength, is near the side wall, which is at the bottom position of the figure. The temperature gradient is larger in the rib-length direction than that in flow direction. The maximum temperature difference between the inner and outer surface is less than 2 K.

Fig. 5(b) shows the wall heat flux distribution on the inner surface of the ribbed wall. The heat flux distribution is more nonuniform than the temperature distribution. Since the heat is transferred from the solid to the fluid. As a result, the blue region means high heat flux and the red one means low heat flux. Two high heat flux regions can be observed between ribs. The first one, which is also the larger one, is near the side wall, which is at the up position of the figure. The other one is near

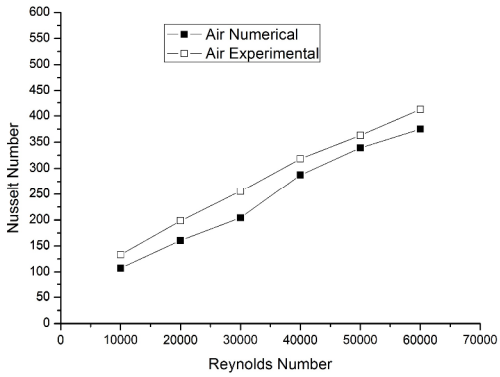

(a) Air

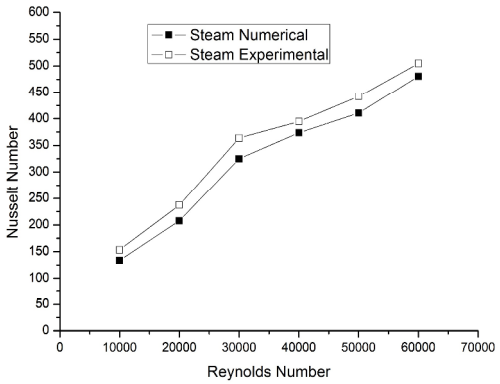

(b) Steam

Fig. 4. The comparison of numerical result and experiment result (Averaged Nusselt number).

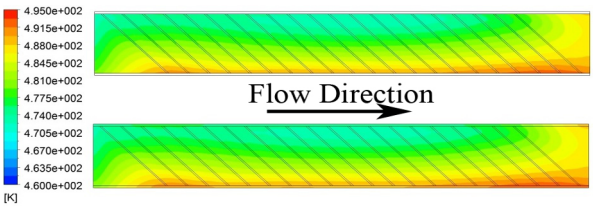

(a) Temperature distribution on the inner surface (up) and outer surface (bottom) of the ribbed wall

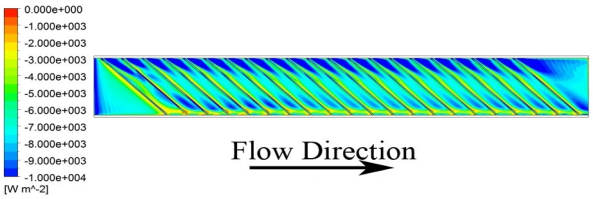

(b) The wall heat flux distribution on the inner surface of the ribbed wall

Fig. 5. Temperature and wall heat flux distribution on ribbed wall (Steam & Re = 60000).

the opposite side wall. However, the heat flux in the region between this region and the nearby side wall is quite low. Other low heat flux region is just near the downstream side of the rib. What's more, the wall in front of the first rib also has low

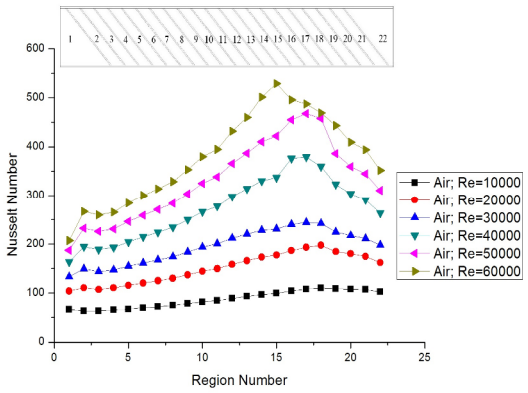

(a) Air

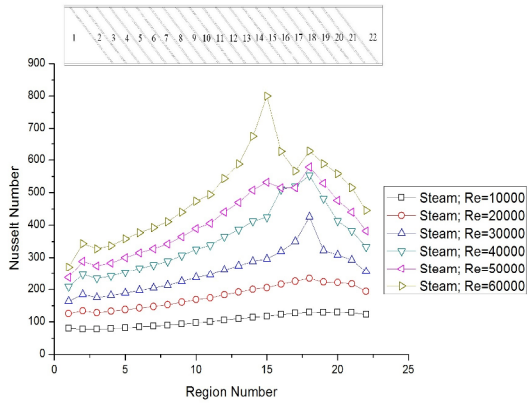

(b) Steam

Fig. 6. The regional averaged Nu on ribbed wall.

heat flux. In comparison, the other walls, which are in front of the rib, have quite high heat flux.

3.2 Comparison of heat transfer performance

To investigate the detailed heat transfer characteristics in different rib space, the ribbed wall was divided into 22 parts, marked as Fig. 6 shows. The No.1 part is the wall between the inlet and the first rib. After that, each part is consists of the rib surface and the rib space between it and the downstream rib. The No. 22 part consists of the No. 22 rib and the rib space between it and the outlet plane.

The regional averaged Nusselt number on the ribbed wall is shown in Fig. 6. Nu for both the air and steam case in the entrance region is lower than the other region, which was also observed by Han [34, 35] and Liu [25]. When the Reynolds number is 10000 and 20000, the Nusselt number trend for both air and steam cases are similar. The Nusselt number reaches the peak value in the No. 18 part and then faces a sudden reduction until the outlet plane. When Re = 30000, 40000 and 50000 for air case, the Nusselt number peak value is reached at No.17. In comparison, the Nusselt number peak value is located at No.18 when the fluid is steam and Re = 30000 40000 and 50000. But it is worth noticing that the peak

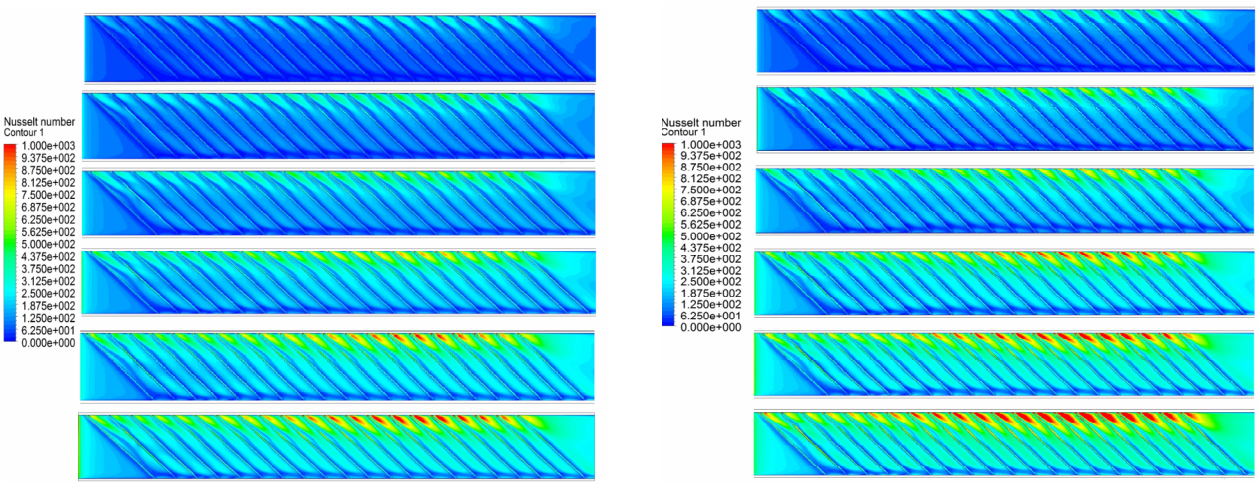

(a) Air (Top to bottom: Re = 10000-60000) (b) Steam (Top to bottom: Re = 10000-60000)

Fig. 7. Nusselt number distribution on ribbed wall (flow direction from the left to right of the figure).

value in this case is obviously larger than that in nearby parts. For the air case, the peak value of Nusselt number is reached at No. 15 when Re = 60000. For the steam case, a slight reduction can be observed from No.16 to No.17 parts for Re = 40000, and a more obvious reduction can be seen from No.15 to No.17 for Re = 50000. When Re = 60000, the peak value is first reached at No.15 and then a large reduction can be observed between the No.15 and No.17 parts. Then the Nusselt number continues to increase and reaches another peak value at No.18 whose value is smaller than the peak value at No.15.

Fig. 7 shows the distribution of Nusselt number on the ribbed wall. The peak value of the Nusselt number is beside the side wall, which is the end of rib that is nearer to the inlet. The minimum value of the Nusselt number appears near the other side wall region and the back surface of the rib. However, the increasing of Reynolds number can gradually enhance the Nusselt number value, especially in the high Nusselt number region. For a certain Reynolds number, the Nusselt number value is also gradually increased when the coolant is steam. Furthermore, the distributions of wall heat flux and Nusselt number are similar. The high wall heat flux position corresponds to the high Nu position. So the wall heat flux distribution is strongly influenced by the heat convection.

3.3 Overall secondary flow vortex core distribution

Fig. 8 shows the overall distribution of secondary flow vortex core for steam in Re = 20000 case. The Secondary flow between Ribs is located below the top surface of the ribs and the Main flow secondary flow 1 is near the side wall above the rib. Since the height of the channel is small compared to the width, the flow in near wall region will be strongly influenced by the main flow fluid. As a result, the Main flow secondary flow 2 is generated by separating from the secondary flow between ribs. It touches the symmetric plane and this part is named as Separation vortex 1. At the same time, a separation vortex, Separation vortex 2, is generated. They finally mix into one vortex, which is named as Mixed separation vortex. Fig. 8(d) shows that the Side wall low speed secondary Flow is generated at the corner which is formed by the rib and side wall due to the separation of secondary flow between ribs from the rib.

Fig. 9 shows the distribution and shape of secondary flow when the coolant is steam and the Reynolds number is 50000. The major characteristics of secondary flow are similar to that when Re = 20000. But the Main flow secondary flow 2 is more greatly influenced by the main flow fluid. As a result, this secondary flow mixes into the Main flow secondary flow 2 in the next rib space. The connection region of the two nearby Main flow secondary flow 2 is above the rib, which can only be observed in the last several ribs when Re = 20000.

3.4 Relation between heat transfer and secondary flow

Fig. 10 shows the heat transfer performance and flow field structure in the entrance region. In Fig. 6 the Nusselt number is lower than that in fully-developed region. In comparison, the Nusselt number distribution in Fig. 10(a) shows that the Nusselt number is quite high when fluid enters the channel. However, the Nusselt number value quickly decreases along the flow direction and maintains a low value until the first rib. The surface streamline on the ribbed wall in Fig. 10(a) indicates that the fluid is not disturbed until it reaches the first rib. The vortex core in Fig. 10(b) also shows that the secondary flow mainly is located in main flow region. In near wall region only a few slim vortex cores can be observed. Even the secondary flow in main flow region cannot extend far into the channel. So it can be concluded that few secondary flows are generated in the near wall region of the entrance, and the disturbance generated by the entrance effect is dissipated quickly so that the disturbance strength is not enhanced here. As a result, the heat transfer in the entrance region is quite low.

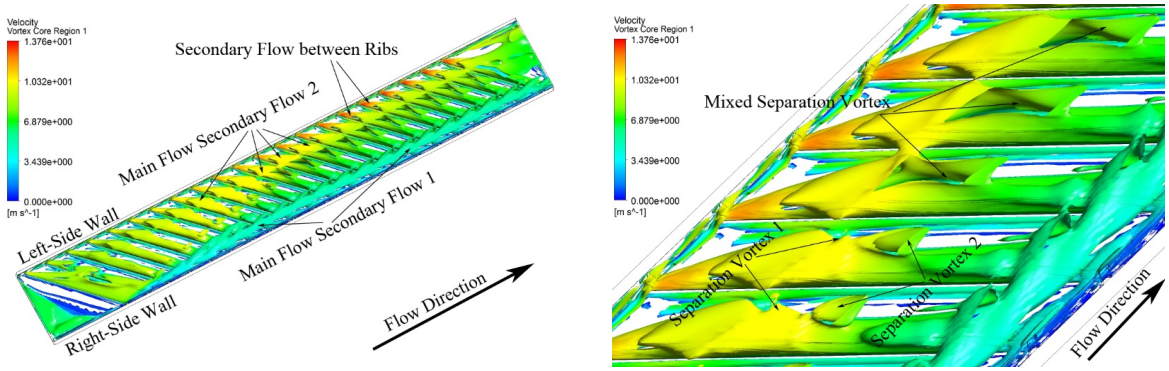

(a) General view (b) Upward view

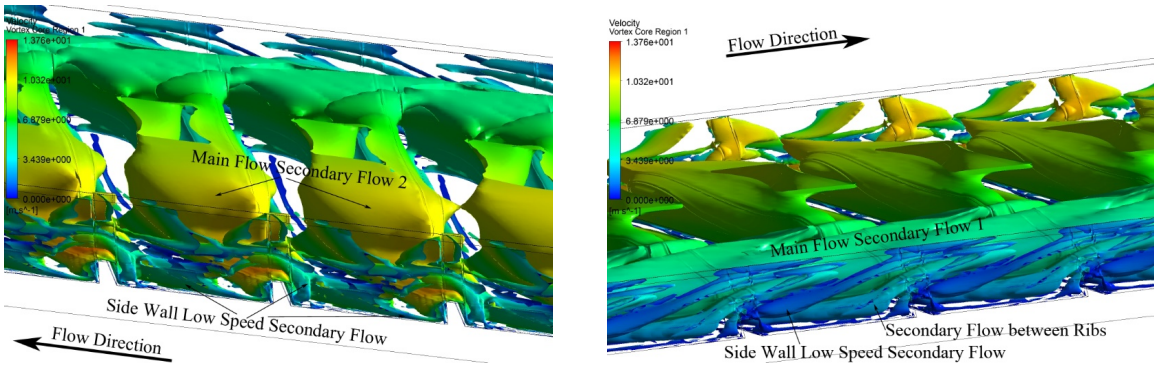

(c) Left-side view (d) Right-side view

Fig. 8. The distribution and shape of secondary flow (Steam, Re = 20000).

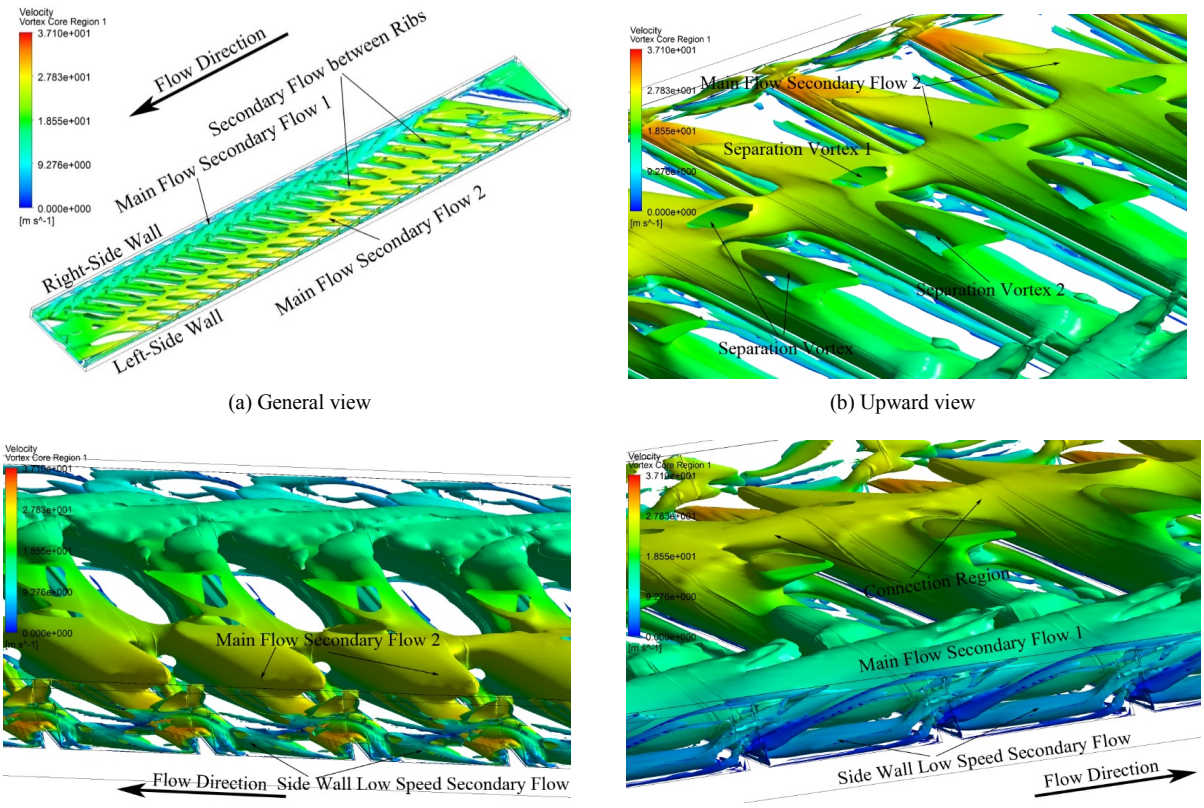

(a) General view (b) Upward view

(c) Left-side view (d) Right-side view

Fig. 9. The distribution and shape of secondary flow (Steam, Re = 50000).

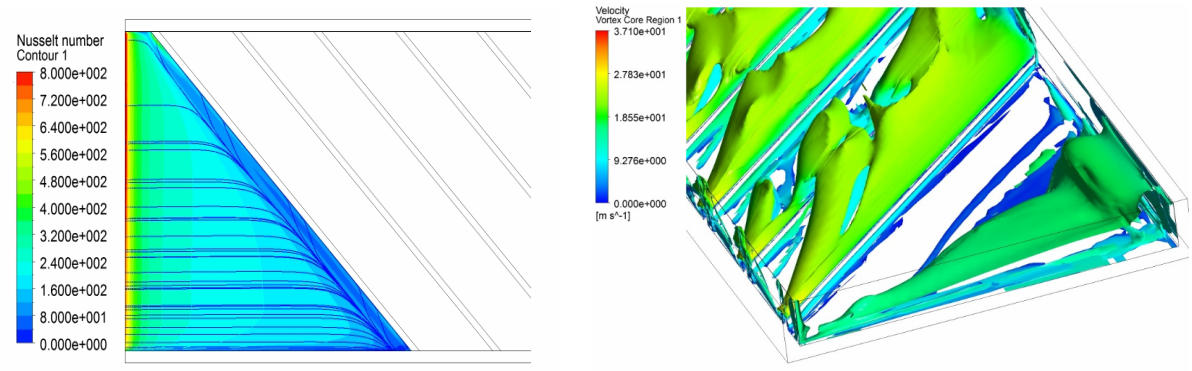

(a) Nusselt number distribution and surface streamline (b) Secondary flow vortex core

Fig. 10. The Nusselt number and secondary flow vortex core distribution in entrance region (Steam, Re = 50000).

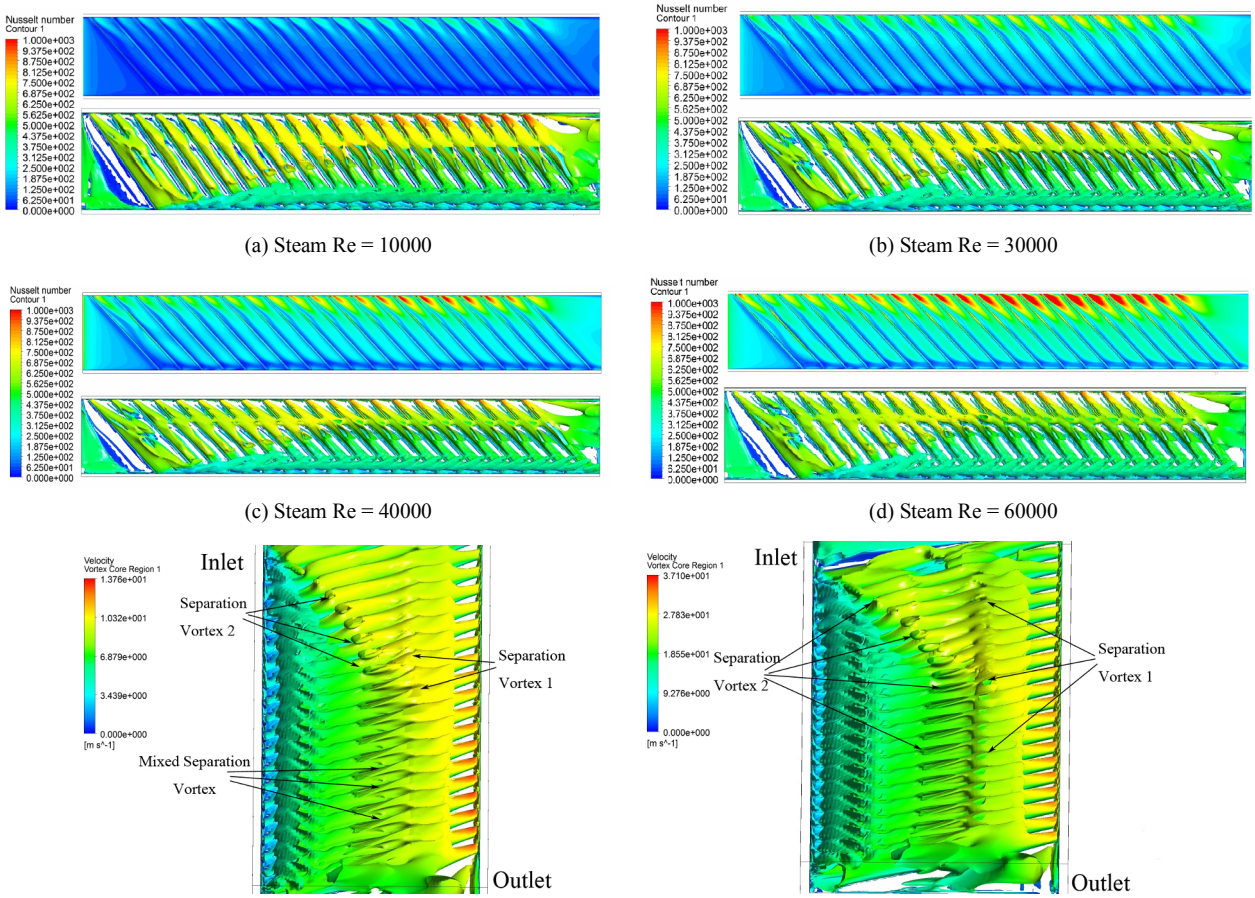

(a) Steam Re = 10000 (b) Steam Re = 30000

(c) Steam Re = 40000 (d) Steam Re = 60000

(e) Relative position of Separation vortex (Steam, Left: Re = 20000, Right: Re = 50000)

Fig. 11. The Nusselt number distribution on the ribbed wall and secondary flow vortex core (Flow direction: left to right).

Fig. 11 shows the comparison of Nusselt number on the ribbed wall and the distribution of secondary flow when the coolant is steam and Re = 10000, 30000 and 60000. The Nusselt number distribution is periodic in each rib space of fully-developed region. In every rib space, the peak value of Nusselt number corresponds to the generation of Secondary flow between ribs. The Nusselt number decreases along the developing direction of Secondary flow between ribs. Even though the Main flow secondary flow 2 is generated near the centerline position of the channel, the Nusselt number in rib space is still low. When Re = 60000, the neighboring Main flow secondary flow 2 are able to connect with each other. However, a relatively high Nusselt number can only be observed at the corresponding position on the rib top surface. That is because the Main flow secondary flow 2 and the connection region of it are both located in main flow region. The connection region is

just at the height of rib top surface and its mix with the downstream Main flow secondary flow 2 can directly enhance the local disturbance strength.

Another obvious characteristic of the Nusselt number is that it varies along the flow direction, which is also clearly shown by Fig. 6. In Fig. 11 the transverse relative position of Separation vortex 1 is not changed. However, the transverse relative position of Separation vortex 2 changes largely in every working condition. The distance between them is reduced in flow direction. When Re = 10000, 20000 and 30000, these two vortexes mix together into one vortex after the No. 11 rib space. However, when Re = 40000, 50000 and 60000, which is shown in Figs. 9 and 11, these two vortexes are getting smaller and will never mix together at all. In these three cases, it will begin to move away from each other after the distance between them reaches the minimum value. The peak value location of Nusselt number, which is shown in Fig. 6, is the same as the location when the distance between the separation vortexes is small. When the distance is getting larger, the Nusselt number will also be reduced. So there may be some relationship between local heat transfer and the relative position of separation vortex. The generation of separation vortex can enhance the local disturbance strength and then enhance the heat transfer strength in downstream region along the rib. As a result, the green region in Figs. 11(c) and (d) in these location is a little larger than that in other region.

The blue region, which indicates low heat transfer strength, is near the side wall, which is the bottom side of the figure. This region is located just between the Side wall low speed secondary flow and the Secondary flow between ribs. Since no near wall secondary flow provides additional disturbance, the local heat transfer strength is lower than the nearby region. In comparison, the Nusselt number in the region between the minimum Nu region and side wall is quite high due to the influence of the Side wall low speed secondary flow.

The separation of secondary flow can directly enhance the local heat and mass transfer strength. Separation vortex 2 is separated from the secondary flow between ribs. According to the analyses above, the averaged local heat transfer strength is inversely proportional to the distance between these two separation vortexes. Since the channel is quite wide, the separation vortex and the mixed vortex can also both enhance the mass transfer in transverse direction. The approaching and mix of the separation vortexes can strengthen the influence of them on mass transfer at centerline region and enhance the local heat transfer strength.

3.5 Secondary flow structure comparison of air and steam

Fig. 12 shows the comparison of secondary flow vortex core structure when fluid is air or steam. From Figs. 12(a) and (b), the secondary flow structure in the entrance region is similar when fluid is air or steam. However, this situation changes when the flow is in the fully-developed region. When Re = 30000, the shape of mixed separation vortex is different for these two kinds of fluid. When the fluid is air, the cross-section shape of mixed separation vortex is like a figure "8" shape, which is narrow in the middle. However, the shape of mixed separation vortex is like a zero "0" shape, which is much wider in the middle. When Re = 60000, the distance between the two separation vortexes is obviously different in the same position for different fluids. When the fluid is air, the distance is larger than that of steam. In conclusion, the distance between the two separation vortexes is smaller for steam than that in the same position for air.

4. Conclusions

Conjugate heat transfer simulation is used to predict the overall temperature, wall heat flux and Nusselt number distribution of a 45 deg ribbed rectangular channel heated by large-current and low-voltage heating method. A heat source was located in the solid domain to simulate the actual heating method. The heat conduction process was taken into consideration. The vortex core of secondary flow was shown to illustrate the heat transfer performance. Some essential conclusions are drawn below:

(1) The temperature distribution is similar for both the inner and outer surface of the ribbed wall. The temperature changes quite a lot along the transverse direction. For a certain rib and the region before the downstream rib, the maximum temperature is at the rib end, which is near the inlet plane and the minimum temperature is at the opposite side. The maximum temperature difference between the inner and outer surface of a certain position is less than 2 K.

(2) The distribution of wall heat flux on the inner surface of the ribbed wall is periodic. Heat is uniformly generated in the solid channel wall using the large-current and low-voltage heating method. The non-uniform wall heat flux and Nusselt number distribution are similar in trend, which indicates that heat is obviously transferred to the well-cooled region. The difference between maximum and minimum value of wall heat flux is about 10000 W/m^2. As a result, heat conduction should be considered in the numerical simulation when this method is adopted in the channel with relative thick wall.

(3) The secondary flow vortex core is similar under the same Reynolds number no matter the coolant. There are two "Main flow secondary flow" in the main flow region. The development of Main flow secondary flow 1 is limited by the channel height scale, and its size changes little along the flow direction. The Main flow secondary flow 2 is formed from the Secondary flow between ribs. The appearance of connection region between nearby Main flow secondary flow 2 can indicate the peak value of Nusselt number on rib top surface.

(4) Two Separation vortexes are generated due to the influence of main flow fluid field. These vortexes will mix together into one vortex when Reynolds number is less than 30000. The relative distance between them at high Reynolds number conditions can illustrate the change of regional averaged Nus-

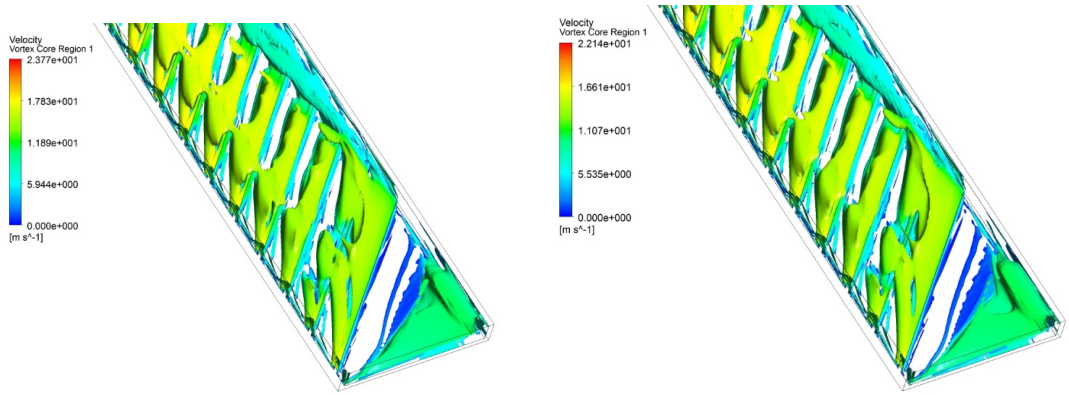

(a) Entrance region (Re = 30000, left: Air; right: steam)

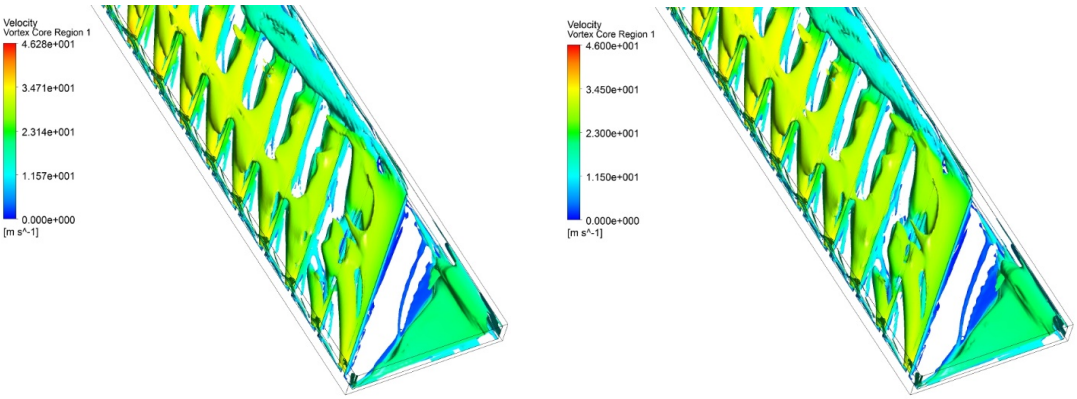

(b) Entrance region (Re = 60000, left: Air; right: steam)

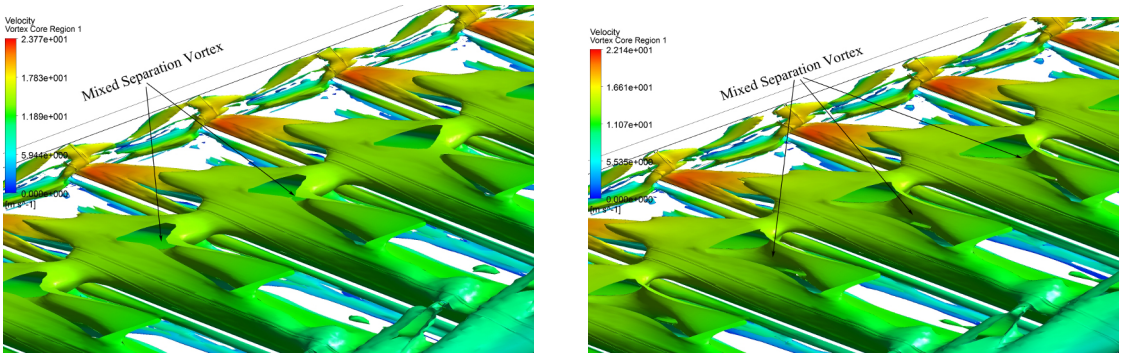

(c) Fully-developed region (Re = 30000, left: Air; right: steam)

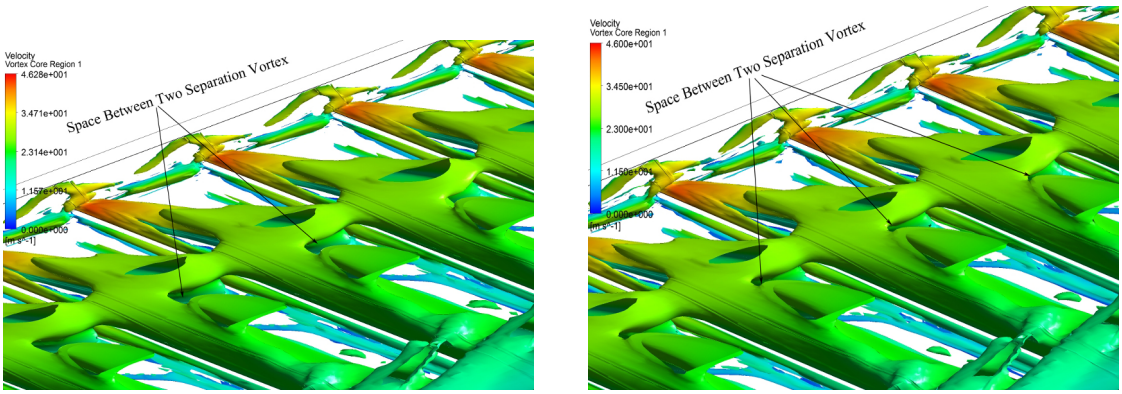

(d) Fully-developed region (Re = 60000, left: Air; right: steam)

Fig. 12. The comparison of secondary flow structure for air and steam.

selt number: The smaller the distance, the higher the regional averaged Nusselt number. That is because the separation vortexes can enhance the mass transfer between the near wall region and the main flow region. The lower distance can indicate higher mass transfer strength. The distance between the two separation vortexes is smaller for steam than that in the same position for air.

(5) The generation, separation and mixing of secondary flow can directly enhance the local heat transfer strength. The influence of near wall secondary flow on heat transfer enhancement is reduced along its path when no separation and interaction of other secondary flow take place. For a large width to height ratio channel, more disturbance should be added at the region below the "Main flow secondary flow 1" to enhance the possibility of the generation of new secondary flow and the mixing of secondary flow in order to further enhance the local heat transfer strength.

Acknowledgment

This work supported by Research Program supported by the National Natural Science Foundation of China (No.50806059) and the Innovative Research Team in University of Ministry of Education of China (IRT1280), China.

Nomenclature

h	: Heat transfer coefficient, W/(m^{2}K)
H	: Channel height, mm
e	: Rib height, mm
e/D	: Ratio of rib height and hydraulic diameter of channel
D_h	: Hydraulic diameter of channel, mm
k	: Thermal conductivity, W/(mK)
L	: Streamwise length of the channel, mm
$L1$	: The distance from inlet to the 1st rib
Nu	: Nusselt number
Nu_0	: Nusselt number in fully-developed turbulent tube flow
P/e	: Ratio of rib pitch to rib height
Pr	: Prandtl number
q	: Heat flux, W/m^2
Re	: Reynolds number
T_b	: Local bulk temperature of fluid, K
T_w	: Local wall temperature, K
V	: Velocity, m/s
W	: Width of the channel, mm
μ	: Fluid dynamic viscosity
ρ	: Fluid density
λ	: Eigen-values of the velocity gradient tensor
Ω	: Anti-symmetric components of velocity gradient tensor
S	: Symmetric components of velocity gradient tensor

References

[1] J. C. Han, J. S. Park and C. K. Lei, Heat transfer enhancement in channels with turbulence promoters, *ASME J. Engng. Gas Turbines Pwr.*, 107 (1985) 628-635.

[2] J. C. Han and J. S. Park, Developing heat transfer in rectangular channels with rib turbulators, *Int. J. Heat Mass Tran.*, 31 (1) (1988) 183-195.

[3] J. S. Park, J. C. Han, Y. Huang and S. Ou, Heat transfer performance comparisons of five different rectangular channels with parallel angled ribs, *Int. J. Heat Mass Tran.*, 35 (11) (1992) 2891-2903.

[4] J. C. Han, Y. M. Zhang and C. P. Lee, Influence of surface heat flux ratio on heat transfer augmentation in square channels with parallel, crossed, and V-shaped angled ribs, *J. Turbomach.*, 114 (4) (1992) 872-880.

[5] P. R. Chandra, M. L. Fontenot and J. C. Han, Effect of rib profiles on turbulent channel flow heat transfer, *J. Therm Heat Tran.*, 12 (1) (1998) 116-118.

[6] Y. J. Jang, H. C. Chen and J. C. Han, Flow and heat transfer in a rotating square channel with 45 deg angled ribs by Reynolds stress turbulence model, *J. Turbomach.*, 123 (1) (2001) 124-132.

[7] G. Rau, M. Cakan, D. Moeller and T. Arts, The effect of periodic ribs on the local aerodynamic and heat transfer performance of a straight cooling channel, *J. Turbomach.*, 120 (2) (1998) 368-375.

[8] R. Kiml, S. Mochizuki and A. Murata, Effects of rib height on heat transfer performance inside a high aspect ratio channel with inclined ribs, *J. Enhanced Heat Trans.*, 10 (4) (2003) 431-443.

[9] C. H. Liu and T. N. H. Chung, Forced convective heat transfer over ribs at various separation, *Int. J. Heat Mass Tran.*, 55 (19-20) (2012) 5111-5119.

[10] D. N. Ryu, D. H. Choi and V. C. Patel, Analysis of turbulent flow in channels roughened by two-dimensional ribs and three-dimensional blocks, Part II: Heat Transfer, *Int. J. Heat Fluid Flow*, 28 (5) (2007) 1112-1124.

[11] S. Leonardi, P. Orlandi, L. Djenidi and R. A. Antonia, Structure of turbulent channel flow with square bars on one wall, *Int. J. Heat Fluid Flow*, 25 (3) (2004) 384-392.

[12] J. Schabacker, A. Bolcs and B. V. Johnson, PIV Investigation of the flow characteristics in an internal coolant passage with two Ducts connected by a sharp 180° bend, *International Gas Turbine and Aeroengine Congress and Exposition 1998*, Stockholm, Sweden (1998) ASME Paper 98-GT-544.

[13] M. Schüler, F. Zehnder, B. Weigand, V. J. Wolfersdorf and S. O. Neumann, The effect of turning vanes on pressure loss and heat transfer of a ribbed rectangular two-pass internal cooling channel, *J. Turbomach.*, 133 (2) (2010) 021017-021017.

[14] X. Liu, Z. Tao, S. Ding and G. Xu, Experimental investigation of heat transfer characteristics in a variable cross-sectioned two-pass channel with combined film cooling holes and inclined ribs, *Appl. Therm. Eng.*, 50 (1) (2013) 1186-1193.

[15] T. M. Liou, S. W. Chang, S. P. Chan and Y. S. Liu, PIV measurements in a two-pass 90-deg ribbed-wall parallelo-

gram channel, *Proceedings of ASME Turbo Expo 2014*, Dusseldorf, Germany (2014) ASME GT2014-25248.

[16] S. Kubacki, J. Rokocki and E. Dick, Hybrid RANS/LES of flow in a rib-roughened rotating channel, *Proceedings of ASME Turbo Expo 2014*, Dusseldorf, Germany (2014) ASME GT2014-26194.

[17] J. Corman, H gas turbine combined cycle power generation system for the future, *Proc. of Yokohama Gas Turbine Congress*, Yokohama, Japan (1995).

[18] I. Fukue, A new generation of advanced gas turbine, *Yokohama International Gas Turbine Congress*, Yokohama, Japan (1995).

[19] B. Facchini, G. Ferrara and L. Innocenti, Blade cooling improvement for heavy duty gas turbine: the air coolant temperature reduction and the introduction of steam and mixed steam/air cooling, *Int. J. Therm. Sci*., 39 (2000) 74-84.

[20] Sanjay, O. Singh and B. N. Prasad, Influence of different means of turbine blade cooling on the thermodynamic performance of combined cycle, *Appl. Therm. Eng*., 28 (2008) 2315-2326.

[21] S. Kumar and O. Singh, Thermodynamic performance evaluation of gas turbine cycle with transpiration cooling of blades using air vis-à-vis steam, *Proceedings of the Institution of Mechanical Engineers, Part A: Journal of Power and Energy*, 224 (2010) 1039-1047.

[22] H. Nomoto, A. Koga, S. Ito, Y. Fukuyama, F. Otomo, S. Shibuya, M. Sato, Y. Kobayashi and H. Matsuzaki, The advanced cooling technology for the 1500°C class gas turbines: steam-cooled vanes and air-cooled blades, *ASME J. Eng. Gas Turbines Power*, 119 (1997) 624-632.

[23] J. Liu, J. Gao and T. Gao, An experimental investigation of heat transfer characteristics in a steam-cooled square channel with rib turbulators, *Proceedings of ASME Turbo Expro 2011*, ASME, Vancouver, Canada (2011) 1-6.

[24] J. Liu, J. Gao and T. Gao, Forced convection heat transfer of steam in a square ribbed channel, *JMST*, 26 (2012) 1291-1298.

[25] J. Liu, J. Gao, T. Gao and X. Shi, Heat transfer characteristics in steam-cooled rectangular channels with two opposite rib-roughened walls, *Appl. Therm. Eng.*, 50 (2013) 104-111.

[26] L. Shui, J. Gao, L. Xu and X. Wang, Numerical investigation of heat transfer and flow characteristics in a steam-cooled square ribbed duct, *Proceedings of ASME Turbo Expo 2010: Power for Land, Sea and Air*, ASME, Glasgow, UK (2010) 1-9.

[27] L. Shui, J. Gao, X. Shi and J. Liu, Effect of duct aspect ratio on heat transfer and friction in steam-cooled ducts with 60° angled rib turbulators, *Exp. Therm. Fluid. Sci*., 49 (2013) 123-134.

[28] J. Y. Gong, T. Y. Gao and G. J. Li, Heat transfer and friction characteristics in steam cooled rectangular channels with rib turbulators, *JMST*, 28 (1) (2014) 357-364.

[29] J. Y. Gong, T. Y. Gao and G. J. Li, Contrastive experimental study on heat transfer and friction characteristics in steam cooled and air cooled rectangular channels with rib turbulators, *JMST*, 28 (9) (2014) 3845-3854.

[30] J. N. Zhu, T. Y. Gao, J. Li, G. J. Li and J. Y. Gong, The Effect of vortex core distribution on heat transfer in steam cooling of gas turbine blade internal ribbed channels, *Proceedings of ASME Turbo Expo 2014*, Dusseldorf, Germany (2014) ASME GT2014-25324.

[31] S. J. Kline and F. McClintock, Describing uncertainties in single-sample experiments, *Mechanical Engineering*, 75 (1953) 3-8.

[32] D. Walker and J. Zausner, RANS evaluations of internal cooling passage geometries: Ribbed passages and a 180 degree bend, *Proceedings of ASME Turbo Expo 2007*, Montreal, Canada (2007) ASME GT2007-27830.

[33] J. Jeong and F. Hussain, On the identification of a vortex, *J. Fluid Mech*., 285 (1995) 69-94.

[34] T. S. Griffith, L. Al-Hadhrami and J. C. Han, Heat transfer in rotating rectangular cooling channels (AR = 4) with angled ribs, *J. Heat Trans*., 124 (4) (2002) 617-625.

[35] M. Al-Qahtani, H. C. Chen and J. C. Han, A numerical study of flow and heat transfer in rotating rectangular channels (AR = 4) with 45 deg rib turbulators by Reynolds stress turbulence model, *J. Heat Trans*., 125 (1) (2003) 19-26.

Tieyu Gao currently works at Xi'an Jiaotong University. His major research includes two-phase flow in turbomachinery and the air and steam cooling technology of gas turbine.